



HAL
open science

Uncertainty analysis and validation of the estimation of effective hydraulic properties: application to green roof substrate

Arnaud Mesgouez, Samuel Buis, Stéphane Ruy, Gaëlle Lefeuvre-Mesgouez

► **To cite this version:**

Arnaud Mesgouez, Samuel Buis, Stéphane Ruy, Gaëlle Lefeuvre-Mesgouez. Uncertainty analysis and validation of the estimation of effective hydraulic properties: application to green roof substrate. 2013. hal-00793526v1

HAL Id: hal-00793526

<https://hal.science/hal-00793526v1>

Preprint submitted on 22 Feb 2013 (v1), last revised 24 Mar 2014 (v4)

HAL is a multi-disciplinary open access archive for the deposit and dissemination of scientific research documents, whether they are published or not. The documents may come from teaching and research institutions in France or abroad, or from public or private research centers.

L'archive ouverte pluridisciplinaire **HAL**, est destinée au dépôt et à la diffusion de documents scientifiques de niveau recherche, publiés ou non, émanant des établissements d'enseignement et de recherche français ou étrangers, des laboratoires publics ou privés.

Uncertainty analysis and validation of the estimation of effective hydraulic properties: application to green roof substrate

A. Mesgouez^{a,b,*}, S. Buis^{b,a}, S. Ruy^{b,a}, G. Lefeuvre-Mesgouez^{a,b}

^a*Université d'Avignon et des Pays de Vaucluse, UMR1114 EMMAH, Faculté des Sciences, F-84000 Avignon, France*

^b*INRA, UMR1114 EMMAH, F-84914 Avignon, France*

Abstract

The determination of the hydraulic properties of heterogeneous soils or porous media remains challenging. In the present study, we focused on determining the effective properties at the Darcy scale of green roof substrates (GRS), highly heterogeneous porous media used in the construction of buildings.

Preliminary, experimental measurements of the hydraulic properties of each component of the GRS, namely bark compost and pozzolan, were obtained. The properties of the effective medium, representing an equivalent homogeneous material to the GRS, had been determined numerically by simulating a water flow in a 3D representation of the GRS, under steady-state scenarios, using its components properties. One of the major aspects of this study was to take into account the uncertainties of these properties in the computation and evaluation of the effective properties. This was done using a bootstrap method.

Numerical evaporation experiments were conducted both on the heterogeneous and on the effective homogeneous materials to evaluate this upscaling approach. First, the impact of the uncertainties of the components properties on the simulated water matric potential was found to be high for the heterogeneous material configuration. Second, it was shown that the use of the upscaling method led to a reduction of this impact. Finally, the adequacy

*Corresponding author

Email addresses: arnaud.mesgouez@univ-avignon.fr (A. Mesgouez),
sbuis@avignon.inra.fr (S. Buis), ruy@avignon.inra.fr (S. Ruy),
gaelle.mesgouez@univ-avignon.fr (G. Lefeuvre-Mesgouez)

between the means of the simulations for the two configurations confirmed the suitability of the upscaling approach used, even in the case of dynamic scenarios.

The methodology proposed in this study is generic. In our context, it could be applied to optimizing the hydraulic properties of composite porous materials in order to improve the hydraulic functioning of green roof substrates.

Keywords: effective hydraulic parameters, heterogeneous medium, uncertainty estimation, green roof substrate, the Richards equation, bootstrapping method

1. Introduction

Green roofs (GR) are considered to serve a number of beneficial purposes that can help in the management of various environmental problems. Indeed, green roofs have been reported to aid in the reduction of air pollution and of the carbon footprints of cities [1] [2], in the preservation of biodiversity [3], in the improvement of storm water management [4] [5] and, of course, in the improvement of energy efficiency in buildings [6] [7]. With this in mind, a global project focusing on the improvement of habitats was developed by a French consortium involving both research and industrial laboratories. The first aspect of the project was to study the thermal benefits of green roofs [8]. The authors analyzed the impact of green roofs on the energy performance of a single-family house under typical French weather conditions, and proposed several comparisons with conventional roofs. For that purpose they developed an energy balance model adapted to GR specificities. Many green roof substrate parameters involved in the energy balance model, such as thermal conductivity, specific heat capacity, albedo, ... vary as a function of the substrate water content. Therefore the energy balance model should be coupled with a water balance model of the GR to perform a thorough evaluation of the thermal performance of GR. However, in order to develop and parametrize such models, specific focus on water flow processes inside the green roof substrate are needed : this is the topic of the present manuscript.

The green roof substrate, hereafter called substrate or complex substrate, is a composite of compressible materials, namely organic matter (bark compost) used as fertilizer, and of aggregates of volcanic rock (pozzolan) used as rigid skeleton. The GRS is, thus, a highly heterogeneous porous medium,

26 the individual components of which can be characterized. When considering
27 vadoze zone science and hydrology science, green roof heterogeneity can be
28 assessed at three different scales at least (the microscopic, macroscopic and
29 field scales), following a similar methodology to that described by [9] [10] [11]
30 [12]:

- 31 • (i) The first scale of interest (or microscopic scale) is that of individual
32 pores, in which water flow through both materials is described by the
33 Navier-Stokes equations. In this case, spatial variability arises from
34 variations in pore-sizes and pore wall properties across characteristic
35 lengths of a few micrometers.
- 36 • (ii) The second scale of interest from a decision making point of view
37 is the field scale, or in our case the roof or building scale, in order,
38 for instance to compute the global water balance, or to couple water
39 flow and heat fluxes in order to manage building cooling systems using
40 numerical models [4] [6] [8]. These global models require the knowledge
41 of thermal and hydraulic parameters which can then be spatialized at
42 the roof scale. However, at the roof scale, the influence of subscale
43 heterogeneities are not solved by the model. In the case of green roofs,
44 these heterogeneities can be due to the industrial execution of green
45 roofs leading to spatial variability in the density of the GRS, in differ-
46 ences in the relative proportion of compost and pozzolan, and, thus,
47 to variability in thermal and hydraulic parameters. These parameters
48 can only be measured at an intermediate scale.
- 49 • (iii) The third scale of interest (or macroscopic scale) is this interme-
50 diate scale, the characteristic length of which ranges from centimeters
51 to decimeters. This is the scale at which hydraulic and thermic pa-
52 rameters are meaningful and can be measured. It is usually called
53 the Darcy scale for hydraulic properties. The work presented in this
54 manuscript was conducted at this scale.

55 At the Darcy scale, each component of the GRS can be considered as a
56 single-phase continuum, the properties of which are defined by macroscopic
57 parameters (hydraulic conductivity and water retention curves) and by phe-
58 nomenological laws (the Darcy law and the Richards equation). Water flow
59 simulation or water balance computation can be performed on a GRS volume
60 by using a numerical solver of the Richards equation accounting for the spa-
61 tial heterogeneity of the hydraulic properties. The spatial structure of the

62 GRS must be known to distribute the hydraulic properties of both materials
63 on the volume of interest. Solving the Richards equation is very tedious, in
64 this case, since it is a non linear equation applied to multidimensional geom-
65 etry. A simpler approach would be to replace the explicit three-dimensional
66 structure of the GRS volume by a homogeneous medium, the properties of
67 which would take into account the hydraulic properties of each material,
68 in such a way that simulations conducted on both domains would produce
69 similar boundary water fluxes under identical boundary Dirichlet conditions
70 [13]. This approach would lead to equations containing fewer unknowns, and
71 the parametrisation of which would, therefore, be easier to perform (homo-
72 geneous and uniform properties instead of heterogeneous and non-uniform
73 properties), and which would be solved more rapidly and more efficiently.
74 Such a medium and such properties are known, respectively, as an effective
75 medium and effective properties.

76 The first objective of this study was to characterize the effective hydraulic
77 properties of real GRS samples taking into account uncertainties in the deter-
78 mination of the hydraulic properties of its individual components. Due to
79 the recent advances in computing capabilities, numerical approaches are now
80 widely used for the determination of effective properties [14] [15]. The deter-
81 mination of the effective hydraulic properties was performed by means of a
82 series of steady-state numerical simulations. Previous studies carried out on
83 natural soils include [13] [16] or [17], the authors of which estimated the ef-
84 fective hydraulic properties of Albeluvisol, agricultural silt soil or monolithic
85 subsoil, respectively, but did not integrate a complete uncertainty evaluation
86 in their studies. However, the process of estimating the hydraulic proper-
87 ties of a given material include various sources of uncertainty [18] [19] that
88 may significantly affect numerical simulations [20] [21] [22] and, thus, affect
89 the estimation of effective properties or their evaluation using dynamic sce-
90 narios. Therefore, estimating the resulting uncertainties on the estimation
91 of hydraulic properties and their impacts on simulation results is impor-
92 tant to assess the quality of effective properties estimation and to interpret
93 the results. Taking into account all type of uncertainties using for example
94 Monte Carlo error propagation method would be very tedious and difficult
95 since they are numerous and since modelising their probability distribution,
96 including possible dependancies, would be extremely complicated. The boot-
97 strap method is a resampling method, and is recognized to be a simple and
98 efficient way of estimating the probability distribution of a statistic. It can
99 be used to estimate a statistic without it being biased, to evaluate the accu-

100 racy of this estimation and/or to build confidence intervals for this statistic
101 [23] [24]. Here, we propose to evaluate the uncertainty of the hydraulic prop-
102 erties of the equivalent homogeneous medium by taking into account, in the
103 numerical processing, the uncertainties estimated for the hydraulic proper-
104 ties of each component. To that effect, several bark compost and pozzolan
105 samples were studied and the uncertainty of their hydraulic properties were
106 estimated using the bootstrap method.

107 The second objective of this study was to evaluate the effectiveness of
108 the previous upscaling approach with respect to dynamic simulations. Sev-
109 eral authors [15] [25] have previously noted that simulations conducted using
110 effective parameters may differ from simulations conducted with spatially
111 variable parameters, in particular when non-equilibrium flows are involved.
112 An evaluation of the upscaling methodology would, therefore, be required
113 and should be performed by minimizing the occurrence of non-equilibrium
114 flows. In the present study, simulations of a dynamic evaporation process
115 using either the two-component substrate or the effective homogeneous ma-
116 terial were compared, as it was previously shown that non-equilibrium flows
117 are generally absent under evaporation conditions [26]. The comparisons
118 were once again performed by including uncertainties estimated for the hy-
119 draulic properties of both the two-component substrate and the effective
120 homogeneous material.

121 The manuscript is structured as follows. In section 2, the material char-
122 acteristics are described for the two components of the substrate, and the
123 experimental and numerical methodologies for obtaining the hydraulic prop-
124 erties as well as their associated uncertainties are stated. Section 3 presents
125 the numerical tools used to obtain the effective hydraulic properties of the
126 GRS and the uncertainties associated with these properties, and to evaluate
127 the effectiveness of the upscaling approach. In section 4, values and un-
128 certainties obtained for the hydraulic properties of each component of the
129 GRS as well as of the effective medium are presented and discussed. Simu-
130 lation results of dynamic evaporations of the two-component substrate and
131 the effective medium are then presented to evaluate the upscaling approach.
132 Finally, concluding remarks and future research perspectives are briefly out-
133 lined in section 5.

134 **2. Estimation of material properties and associated uncertainties**
135 **from experimental measurements**

136 *2.1. Experimental procedures*

137 The green roof substrate under study was composed of a combination of
138 40% organic material (bark compost) and 60% volcanic material (pozzolan).
139 This combination corresponds to the volumetric GRS proportions which are
140 actually used in an *in situ* environment. Bark compost was provided by an
141 industrial partner and the precise composition of this compost is confidential.
142 Pozzolan materials were extracted in a quarry located in the “Massif Central”
143 mountain in the center of France. Chemical composition of pozzolan was
144 given by the operator of the quarry (SiO_2 : 42–55%; Al_2O_3 : 12–24%; Fe_2O_3 :
145 8 – 20%). The pozzolan grain size distribution was the following: 2/3 of the
146 pozzolan grain diameters ranged from 3 to 6 mm, and 1/3 from 7 to 15 mm.

147 Estimating the hydraulic properties at the Darcy scale required the pre-
148 liminary characterization of the physical and hydraulic properties of both
149 materials under laboratory conditions. The properties of the two materi-
150 als were measured on samples of both materials, and were measured at the
151 same bulk density [$M.L^{-3}$] as they occur in the actual substrate. Since bark
152 compost is a compressible material, contrary to pozzolan, we followed the
153 procedure described hereafter to be certain that the density of pure bark
154 compost samples was the same as the density of bark compost present in the
155 actual composite substrate. The complex substrate was characterized fol-
156 lowing a standard compaction methodology, namely the Proctor compaction
157 test, standard DIN 18127. The sample was struck 6 times by a 4.5 kg Proc-
158 tor hammer from a height of 45 cm in order to obtain adequate compaction.
159 The compacted sample obtained following this methodology, was supposed
160 to be representative of the *in situ* industrial execution of the green roofs [27].
161 By knowing, on the one hand, the apparent bulk density of the substrate
162 and of the pozzolan aggregates and, on the other hand, the solid density of
163 bark compost and of pozzolan, we extrapolated the apparent bulk density
164 of bark compost in the actual composite substrate. Bark compost samples
165 could subsequently be compacted down to this apparent bulk density and
166 their hydraulic properties, i.e. water retention and hydraulic conductivity,
167 could be measured using ad hoc experimental procedures for different water
168 potentials. These hydraulic properties were then modeled for each material
169 by fitting parametric models to these experimental data.

170 The experimental procedures carried out, and the methodology used to
171 estimate the hydraulic properties and the associated uncertainties are de-
172 scribed in the following sections.

173 *2.2. Uncertainty evaluation methodology*

174 Various approximations and errors can be sources of uncertainty when
175 estimating the hydraulic properties of each material. The following typology
176 is proposed to classify these sources of uncertainty:

- 177 • Variability in the properties of samples: owing to the variability of the
178 material samples used in some experiments, or to the fact that some
179 experiments result in the destruction of the samples used, measure-
180 ments of the properties of a material are often replicated using several
181 samples. The number of samples used may have a significant impact
182 on the estimation of the hydraulic properties of a material depending
183 on the level of their individual variability,
- 184 • Errors in experimental data due to (i) approximations performed on
185 length, weight or density measurements, for instance transducer lo-
186 cations, and to (ii) digitalization errors associated with digital data-
187 loggers. These errors can propagate in the estimation of the hydraulic
188 properties as noted by [28],
- 189 • Model errors due to inadequate model assumptions. [15] showed in
190 a numerical case study that the validation of the upscaling process
191 required a highly flexible hydraulic law model,
- 192 • Fitting errors: in the event of a low number of experimental data, the
193 level of uncertainty of the parameters obtained using parametric models
194 fitted to the experimental data may be very high, even in case of slight
195 variability in the properties of the samples and of slight measurement
196 errors.

197 We used the bootstrap method [23] [24] to estimate the resulting un-
198 certainties on the hydraulic properties and to evaluate their impacts on the
199 simulation results. This method can be used to estimate a statistic without
200 it being biased, to evaluate the accuracy of this estimation and/or to build
201 confidence intervals for this statistic. In the present study, the statistics
202 computed were the parameters of the laws describing hydraulic properties.

203 In the following, we describe the principle of non-parametric bootstrapping
204 which is relatively simple. Let us consider the observation sample obtained
205 for the computation of the statistic, in our case a set of water retention or
206 conductivity measurements associated with water potential values. These
207 observations must be independent and identically distributed to ensure the
208 convergence of the method. N artificial samples, of the same size as the
209 original observation sample, are created by sampling in it with replacement.
210 They are called bootstrap samples. The statistical value is computed for
211 each of these bootstrap samples. Its probability distribution is then approx-
212 imated using the histogram of the N computed statistical values. In other
213 words, the actual variability of the statistic is estimated using the observed
214 variability of the whole of the samples obtained by resampling. Of course,
215 this kind of methodology does not take into account the problem of model
216 error, of large biases or of samples non representative of the population, al-
217 though it produces accurate descriptions of uncertainties under reasonable
218 assumptions and a lower bound of the actual uncertainty level.

219 *2.3. Determination of solid density and apparent bulk density of compost and* 220 *pozzolan*

221 Samples were crunched, sieved at $315\ \mu\text{m}$ and air dried in the oven for 24
222 h at $105\ ^\circ\text{C}$. Solid particles were then placed in the measurement chamber
223 of a He pycnometer and solid bulk density was determined using the Boyle
224 law [29]. The apparent bulk density of pozzolan aggregates was measured
225 on replicates with diameters varying from 7 to 15 mm, using Archimede's
226 law and buoyancy measurements in water. The aggregates were previously
227 saturated in water for 24 h [30]. The apparent bulk density of the composite
228 substrate was measured using the core method [29] adapted for compacted
229 and remolded samples. The apparent bulk density of bark compost present
230 within the composite substrate was deduced. All of the measured properties
231 are displayed in Table 1.

232 *2.4. Determination of water retention and associated uncertainties*

233 Water retention measurements were obtained using the suction table for
234 small suctions (0.05, 0.54, 1.03, 2.01, 3.97, 6.91 kPa) and the pressure plate
235 extractors for large suctions (10, 30, 50, 100, 300, 500 and 1500 kPa) [29]. The
236 total number of replicates differed for pozzolan and bark compost materials.

- 237 • Since pozzolan aggregates are a natural material with a high level of
238 variability due to geological variations occurring during their formation,

		Pozzolan aggregate	Complex substrate	Bark compost
Particle density	Mean	3.000	-	1.670
	σ coefficient of variation	0.020 0.7%	- -	0.040 2.4%
Apparent bulk density	Mean	1.520	0.822	0.195
	σ coefficient of variation	0.230 15.1%	0.002 0.2%	0.003 1.5%

Table 1: Mean and standard deviation values of the particle and apparent bulk densities for bark compost, pozzolan aggregate and complex substrate.

239 a large number of replicates were required to counter the effects of
240 this natural heterogeneity. 10 different aggregates were used for each
241 suction point. The aggregates taken for apparent bulk density mea-
242 surements were also used for the 0 kPa suction point. Water saturated
243 aggregates were gently placed onto a fine layer of kaolinite paste to
244 ensure a good contact between aggregate pores and the sand layer (for
245 suction tables) or the porous plate (for pressure plate extractors). A
246 set time for sample equilibration of 3 days was respected.

247 • Bark compost samples were compacted in the laboratory following a
248 standard procedure in order to obtain a predetermined density of com-
249 post into the composite substrate, the variability of which was very low
250 (see Table 1). A low number of replicates were, therefore, required. 5
251 different bark compost samples were used for each suction point. To ac-
252 count for any natural variability in the density of bark compost within
253 the composite substrate, samples were compacted in small cylinders
254 ranging from 0.184 and 0.213 g.cm⁻³. Mean bulk density was 0.200
255 g.cm⁻³, which differs slightly from the theoretical bulk density of com-
256 post within the composite substrate (0.195 g.cm⁻³), due probably to
257 experimental approximations. After initial saturation, samples were
258 placed onto the suction table or porous plate. Kaolinite paste was also
259 used to increase the quality of the capillary connectivity between the

260 sample and the sand layer or porous plate. The time needed for sample
 261 equilibrium was over one week for each suction point and was controlled
 262 by monitoring the water flow out of the pressure chamber.

263 The van-Genuchten model [31] was fitted to the experimental data in order to
 264 obtain the water retention curve, i.e. the relation between $\theta(h, \mathbf{x}, t)$ [$L^3.L^{-3}$]
 265 the volumetric water content and $h(\mathbf{x}, t)$ [L] the water matric potential, as
 266 follows

$$\theta(h, \mathbf{x}, t) = \theta_r + (\theta_s - \theta_r) \times \left[1 + \left(\frac{h(\mathbf{x}, t)}{h_e} \right)^n \right]^{-m} \quad (1)$$

267 where \mathbf{x} [L] are the spatial coordinates, t [T] is the time, θ_r [$L^3.L^{-3}$]
 268 the residual volumetric water content, θ_s [$L^3.L^{-3}$] is the water content at
 269 saturation, h_e [L] is a scale parameter, n [-] and m [-] are shape parameters
 270 with $m = 1 - 1/n$.

271 First, all the measured data were used to estimate the values of the van
 272 Genuchten model parameters for pozzolan and bark compost. Then, uncer-
 273 tainties of these parameters were estimated by bootstrapping measured data
 274 for each suction point. The van-Genuchten model was, thus, fitted N times,
 275 with $N = 500$ in this case, on N datasets obtained by resampling with re-
 276 placement the measured data. The N resampled datasets contained the same
 277 number of measurements as the original samples, in total and for each suction
 278 point. The van-Genuchten model fits were performed using the non-linear
 279 least squares regression taking into account measurement error variances for
 280 each suction point and using the trust-region-reflective minimizer [32].

281 *2.5. Determination of hydraulic conductivity and associated uncertainties*

282 Hydraulic conductivity was measured for pozzolan and bark compost un-
 283 der water-saturated and unsaturated conditions using two different methods.
 284 Hydraulic conductivity at saturation K_{Sat} [$L.T^{-1}$] was measured using a con-
 285 stant head permeameter [33] for pozzolan cores and bark compost samples.
 286 Unsaturated hydraulic conductivity was measured using the Wind evapora-
 287 tion method [28]. Samples used for determining the hydraulic conductiv-
 288 ity at saturation were also used for determining the unsaturated hydraulic
 289 conductivities. As was the case for determining the water retention curve,
 290 the number of replicates differed for pozzolan and bark compost, and were
 291 adapted to the different variability of both materials: 10 replicates were used
 292 for pozzolan and 1 replicate was used for bark compost.

293 Samples of pozzolan were extracted from large blocks (volume of approx-
 294 imately 1 dm^{-3}). Initially, a classification of these blocks was made based
 295 on the visible porosity and the estimated bulk density: an equal number of
 296 “compact” and “porous” blocks in equal quantities were identified. 10 repli-
 297 cates were then cored from both types of blocks. The vertical walls of the
 298 clods were surrounded by heat shrink tubing to avoid preferential water flow
 299 along the walls during measurements.

300 Samples of bark compost were obtained after their compaction up to 0.195
 301 g.cm^{-3} in cylinders. A single replicate was used, since a low experimental
 302 variability was expected as the compaction procedure was accurately per-
 303 formed and led to a very low level of variability in the porosity obtained (see
 304 Table 1).

305 For measuring the unsaturated hydraulic conductivity, pozzolan clods and
 306 bark compost were equipped with sufficient microtensiometers to obtain an
 307 accurate estimation of their hydraulic properties [28]. After sample satura-
 308 tion, water was allowed to evaporate from the upper surface of each core
 309 under laboratory conditions, i.e. conditioned atmosphere at $24 \text{ }^\circ\text{C}$ under at-
 310 mospheric pressure. The base of each core was sealed to prevent downward
 311 flux.

312 The Mualem-van Genuchten model [31] was fitted to the experimental
 313 data to obtain the hydraulic conductivity curve, i.e. the relation between
 314 $K(h, \mathbf{x}, t)$ [$L.T^{-1}$] and $h(\mathbf{x}, t)$

$$K(h, \mathbf{x}, t) = K_{Sat} \cdot \Theta^{0.5}(h, \mathbf{x}, t) [1 - (1 - \Theta^{1/m})^m]^2 \quad (2)$$

315 where

$$\Theta(h, \mathbf{x}, t) = (\theta(h, \mathbf{x}, t) - \theta_r) / (\theta_s - \theta_r) = \left[1 + \left(\frac{h(\mathbf{x}, t)}{h_e} \right)^n \right]^{-m} \quad (3)$$

316 As for water retention, all the measured data were first used to estimate
 317 the values of the Mualem-van Genuchten model parameters for pozzolan and
 318 bark compost. Then, uncertainties linked to the variability of the pozzolan
 319 clod properties were simulated by bootstrapping in the 10 pozzolan clods.
 320 Uncertainties linked to the experimental setup and data processing were dealt
 321 with by bootstrapping in each clod dataset. N datasets, with $N = 500$,
 322 were thus built by resampling with replacement in the 10 pozzolan samples
 323 and within each selected dataset. Since each resampling step maintained a
 324 constant dataset size, N corresponding conductivity curves were, thus, fitted

325 using the Mualem-van Genuchten model on these N datasets. The Mualem-
 326 van Genuchten model fits were performed using the non-linear least squares
 327 regression assuming error homoscedasticity and using the same minimizer as
 328 for the water retention fit.

329 Porosity ϕ of bark compost was measured for a single set of samples. The
 330 uncertainty of the measured saturated hydraulic conductivity could, thus,
 331 be estimated from the variability in the porosity values using the Kozeny-
 332 Carman model [34]. A simple error propagation computed using this model,
 333 assuming a log-normal distribution of K_{Sat} , gave rise to

$$\text{var} [\log(K_{Sat})] = \left(\frac{3 - \phi}{\phi(1 - \phi)} \right)^2 \text{var}(\phi) \quad (4)$$

334 An approximation of the probability distribution of the hydraulic conduc-
 335 tivity of compost was computed by fitting the Mualem-van Genuchten model
 336 to $N = 500$ datasets built by bootstrapping in the experimental dataset.
 337 Each one of the N datasets also included a single value for K_{Sat} randomly
 338 sampled from the uncertainty distribution estimated as described above. The
 339 regression was performed using the same assumptions and methods as for the
 340 regression measured for the hydraulic conductivity of pozzolan.

341 **3. Computation of effective hydraulic parameters**

342 Effective hydraulic parameters were determined by numerically simulat-
 343 ing a water flow, under specific conditions, in a three-dimensional representa-
 344 tion of the heterogeneous material. This required the preliminary solving of
 345 the highly non-linear Richards equation (RE). Simulations were performed
 346 herein with a specific C++ parallelized code.

347 *3.1. C++ parallelized code and simulation configuration*

348 The three-dimensional variably saturated flow modeling was based on the
 349 non-linear Richards equation. The mixed form of RE obtained by combining
 350 the mass conservation law with the generalized Darcy equation was

$$\frac{\partial \theta(h, \mathbf{x}, t)}{\partial t} = \nabla \cdot (K(h, \mathbf{x}, t) \nabla (h(\mathbf{x}, t) + z)) + Q(\mathbf{x}, t) \quad (5)$$

351 where z is the upward vertical coordinate and $Q(\mathbf{x}, t)$ is a sink or/and source
 352 term. Constitutive functions depending on the materials considered link

353 $h(\mathbf{x}, t)$, $\theta(h, \mathbf{x}, t)$ and $K(h, \mathbf{x}, t)$ and close (5). Various initial and boundary
 354 conditions can complete the parabolic system of partial differential equations.

355 Water flow was solved using the mixed form of the Richards equation
 356 for which a perfect mass balance is ensured, see [35] [36] [37] to cite a few.
 357 Spatial discretization was performed using the Galerkin-type linear isopara-
 358 metric finite elements [38] [39]. The modified Picard iteration scheme was
 359 implemented in a fully implicit Euler time discretization. Different conver-
 360 gence criterion could be used, as explained in [40]. An adaptive time step
 361 adjustment was implemented to improve numerical efficiency [37]. Time and
 362 spatial discretizations resulted in the following system of linear equations

$$\left[\frac{[M^{t+1,m}][C^{t+1,m}]}{\Delta t} + [K^{t+1,m}] \right] \{\delta_u^m\} =$$

$$\{F^{t+1,m}\} - \frac{[M^{t+1,m}]}{\Delta t} \{\theta^{t+1,m}\} + \frac{[M^{t+1,m}]}{\Delta t} \{\theta^t\} - [K^{t+1,m}] \{u^{t+1,m}\} \quad (6)$$

363 where t and m denote, respectively, time and inner iteration levels, $u = h + z$
 364 and $\delta_u^m = u^{t+1,m+1} - u^{t+1,m}$, $[M]$ and $[K]$ are the global mass and stiffness
 365 matrixes, F includes the source/sink terms and $[C(h, \mathbf{x}, t)]$ is the specific
 366 moisture capacity function matrix.

367 A C++ object oriented code was developed to solve (6) and to determine
 368 the water matric potential and the water flux at each node/boundary of the
 369 finite element mesh grid for an unsaturated medium. Our numerical results
 370 were found to corroborate analytical results published by [41] [42] or purely
 371 numerical results proposed by [43].

372 Due to the specific composition of the GRS, very fine spatial grids were re-
 373 quired, leading to huge CPU time and storage cost. This major drawback was
 374 overcome by a parallelization of the code [44] [45]. MPI ([http://www.mpi-](http://www.mpi-forum.org/)
 375 [forum.org/](http://www.mpi-forum.org/)) and PETSc (<http://www.mcs.anl.gov/petsc/>) libraries were used
 376 herein to parallelize the C++ sequential code.

377 Numerical simulations were performed on a typical soil core to compute
 378 the effective parameters at the Darcy scale. In our case, the GRS was repre-
 379 sented by a cylinder of the following dimensions: height = 7 cm and diameter
 380 = 15 cm. This cylinder was discretized with 507,553 nodes and 3,216,152
 381 elements. The average length of each edge was approximately 1.5 mm. As
 382 mentioned above, the pozzolan grain size distribution was the following: 2/3
 383 of the pozzolan grain diameters ranged from 3 to 6 mm, and 1/3 from 7 to 15
 384 mm. A specific algorithm was developed to model the geometry and distri-
 385 bution of pozzolan. This algorithm took into account a mesh of the cylinder

386 obtained by GMSH (<http://geuz.org/gmsh/>). Grains of pozzolan were then
387 created by randomly selecting a seed represented by an element of the mesh.
388 The volume of the grain was randomly chosen from the known grain diameter
389 distribution and assumed that the pozzolan grains were spheric. The grains
390 were then iteratively built by randomly selecting and aggregating adjacent
391 elements of the growing irregular seeds until the required grain volumes were
392 reached. Fig. 1 shows a typical mesh used in the simulations.

393 *3.2. Computation of effective parameters and associated uncertainties*

394 The effective parameters were obtained using a steady-state flow sim-
395 ulation, as explained in [13] [14], in the interval $[-10^2, -10^{-2}]$ m, which
396 corresponds to the validity range of the numerical code. The same water
397 matric potential, a Dirichlet type condition, was applied to the upper and
398 the lower boundaries of the cylinder, leading to a constant water matric po-
399 tential throughout the medium in the case of a homogeneous material. The
400 vertical boundaries were impermeable. In order to obtain the hydraulic con-
401 ductivity, the calculated water flux was divided by the surface of the upper
402 boundary. In the case of a heterogeneous medium, the same configuration
403 led to an almost constant water matric potential in the medium, and the so-
404 called effective hydraulic conductivity of the composite substrate was equal
405 to the average water flux density across the horizontal boundaries. The water
406 retention was calculated for each element with the computed values of nodal
407 matric potential. These conductivity and water retention values were relative
408 to the matric potential value fixed at the boundaries, even if local gradients of
409 matric potential were present within the heterogeneous medium. The compu-
410 tation was, thus, repeated for several water matric potential values in order
411 to fit the conductivity and retention curves. For each water matric potential
412 value relative to the boundary conditions, the following question arose: how
413 to be “sure” that the steady-state flow was reached? The lower water flux
414 was compared to the upper flux and both were calculated at each time point.
415 When relative differences *i*) between two successive time iterations for each
416 water flux and *ii*) at time t between the upper and lower flux became lower
417 than $\epsilon/10$, where ϵ was the required precision of the inner iteration scheme,
418 the simulation was stopped. $\epsilon = 1e - 4$ was used here.

419 In order to take into account uncertainties in the hydraulic properties of
420 pozzolan and compost, the computation of the effective hydraulic conductiv-
421 ity and water retention for each water matric potential value was repeated for
422 a single set of pozzolan and compost properties randomly sampled from their

423 uncertainty distributions. The spatial distribution of the pozzolan grains in
424 the mesh was different for each repetition and was generated randomly as
425 explained above. The sampling of pozzolan and compost properties was per-
426 formed independently for each water matric potential value. The choice of
427 the number and values of water matric potential points and the number of
428 replicates for each water matric potential value, directly affected the compu-
429 tational cost of the estimation of the effective properties and their level of un-
430 certainty. An optimal experimental design technique was used to guide these
431 choices. A D-optimal criterion [46] was computed for fitting the Mualem-van
432 Genuchten and the van Genuchten models. The aim was to minimize this
433 D-criterion which is the determinant of the error covariance matrices of the
434 models parameters. Several contrasted water matric potential distributions
435 of points were considered in the bounded interval $[-10^2, -10^{-2}]$ m : regular
436 distribution, log-regular distribution and quantiles of beta distributions to
437 concentrate points on the left, the right or the center of the interval. The
438 log-regular distribution appeared to be the best compromise with respect to
439 the criterion values computed for both models for a number of water matric
440 potential values. Then, an optimisation of the ratio between the number
441 of water matric potential points and the number of replicates, for a given
442 computational cost corresponding to 200 simulations, was computed with
443 this log-regular distribution. In the end, the D-optimal design, among those
444 tested, was a log-regular repartition of 4 water matric potential points with
445 50 replicates.

446 Similarly to what was done for estimating individual materials proper-
447 ties, all the measured data were first used to estimate the effective material
448 properties. Uncertainty distributions of the effective properties were then
449 obtained by bootstrapping the data computed for all replicates within each
450 water matric potential values and fitting the Mualem-van Genuchten and
451 van Genuchten models to each of these $N = 500$ resampled datasets. The
452 fits were performed using the non-linear least squares regression by taking
453 into account the measured error variances computed for each water matric
454 potential value and using the minimizer described in section 2.4. For the
455 Mualem-van Genuchten model fit, prior information on K_{sat} was considered
456 to regularize the fitting problem. This prior information was modeled as a
457 bounded gaussian distribution. Its bounds were defined as the minimum and
458 maximum of the theoretical Wiener bounds (see section 4.2) at 0 m water
459 matric potential value. Its mean was set to the middle of this interval and
460 its standard deviation to the quarter of its length.

461 *3.3. Evaluation of the upscaling approach under dynamic evaporation*

462 Reliability and accuracy of the estimation procedure of the effective pa-
463 rameters were evaluated using dynamic scenarios. Our aim, here, was to
464 cross-check the upscaling and the bimaterial approaches by simulating the
465 evolution of water matric potential versus time, for various points of the soil
466 core described in section 3.1. A time-variable flux of evaporation ranging
467 from 1.9 mm.d^{-1} to 0.9 mm.d^{-1} was applied to the top surface of the soil
468 core at $z = 0$. The values of the time-variable flux were representative for
469 usual experimental conditions of the Wind evaporation method. The other
470 boundaries were impermeable. The initial condition was that of a quasi-
471 saturated medium with $h(\mathbf{x}, t = 0) = -9.5 \text{ cm}$ for all depths. For $h = -100$
472 m, the flux type boundary conditions were switched to the Dirichlet condi-
473 tions. The simulations lasted 10 days to ensure a greater evaporation and
474 a switch from flux to the Dirichlet conditions at the boundary of the upper
475 part of the soil core.

476 200 simulations were performed for the bimaterial configuration and for
477 the equivalent homogeneous material, by randomly sampling the correspond-
478 ing hydraulic properties in their uncertainty distributions. For the bimaterial
479 configuration, a different spatial distribution of the pozzolan grains in the
480 mesh was randomly generated for each simulation. For each simulation, 4
481 sets of 5 points were considered at 4 different depths in order to monitor the
482 matric potentials. The vertical coordinates were: $z = 0 \text{ cm}$, $z = -0.2 \text{ cm}$,
483 $z = -1.1 \text{ cm}$ and $z = -4.8 \text{ cm}$. For each depth, the arithmetic mean values
484 of matric potential were computed on the 5 points. The distribution of these
485 mean values obtained for the bimaterial configuration were then compared
486 to the distribution obtained for the equivalent homogeneous configuration at
487 each depth.

488 **4. Results and discussion**

489 *4.1. Water retention and hydraulic conductivity curves of pozzolan and com-
490 post*

491 The resulting uncertainty distributions of the water retention for pozzolan
492 and compost are presented in Figs. 2. The estimated values of the van
493 Genuchten model parameters for compost and pozzolan and the standard
494 deviations of the associated uncertainty distributions are displayed in Table
495 2.

		θ_r	θ_s	h_e	n
Compost	Estimat. value	$8.66e^{-2}$	$5.55e^{-1}$	$7.47e^{-3}$	1.22
	σ	$5.92e^{-3}$ (6.9%)	$1.27e^{-2}$ (2.3%)	$1.63e^{-3}$ (21.8%)	$1.01e^{-2}$ (0.8%)
Pozzolan	Estimat. value	0(<i>fixed</i>)	$3.53e^{-1}$	$5.88e^{-3}$	1.29
	σ	0(<i>fixed</i>)	$1.63e^{-2}$ (4.6%)	$2.05e^{-3}$ (34.9%)	$1.11e^{-2}$ (0.9%)
Effective material	Estimat. value	$3.81e^{-2}$	$4.35e^{-1}$	$6.71e^{-3}$	1.26
	σ	$7.17e^{-4}$ (1.9%)	$1.36e^{-2}$ (3.1%)	$1.04e^{-3}$ (15.5%)	$2.74e^{-3}$ (0.2%)

Table 2: Estimated values and associated uncertainties of the van Genuchten model parameters for water retention of compost, pozzolan and effective material.

496 The resulting uncertainty distributions of the hydraulic conductivity for
497 pozzolan and compost are presented in Figs. 3. The estimated values of the
498 Mualem-van Genuchten model parameters for compost and pozzolan and the
499 standard deviations of the associated uncertainty distributions are displayed
500 in Table 3.

501 4.1.1. Comments on the water retention results

502 The water retention measurements of pozzolan were widely spread near
503 saturation. High standard deviations for water content, $0.13 \text{ m}^3/\text{m}^3$ to 0.14
504 m^3/m^3 , were obtained for matric potential values greater than -10^{-2} m .
505 These decreased to a typical value of $0.03 \text{ m}^3/\text{m}^3$ in the central part of the
506 water retention curve and were under $0.007 \text{ m}^3/\text{m}^3$ for the lowest ($h < -10$
507 m) matric potential values. According to the Jurin law, water content near
508 saturation is determined by the proportion of larger pores (up to 1 mm in
509 diameter) that can be found in pozzolan aggregates. Due to the small size of
510 the aggregates (diameter of about 5 mm) used in the present study, the pro-
511 portion of macropores was highly variable from one aggregate to the other,
512 which explains the high variability of the water content near saturation. For
513 lower matric potential values, the water content variability of pozzolan aggre-
514 gates may be attributed to factors involved in pozzolan formation. Indeed,
515 pozzolan is a porous siliceous pyroclastic rock, the porosity of which is created

		K_{Sat}	h_e	n
Compost	Estimat. value	$3.04e^{-3}$	$9.72e^{-3}$	1.12
	σ	$1.03e^{-4}$ (3.4%)	$2.79e^{-4}$ (2.9%)	$8.87e^{-3}$ (0.8%)
Pozzolan	Estimat. value	$6.94e^{-6}$	$6.01e^{-1}$	1.02
	σ	$7.95e^{-6}$ (114.6%)	$9.90e^{-1}$ (164.7%)	$9.64e^{-3}$ (0.9%)
Effective material	Estimat. value	$9.36e^{-4}$	$2.28e^{-2}$	1.05
	σ	$8.91e^{-5}$ (9.5%)	$8.01e^{-4}$ (3.5%)	$1.91e^{-3}$ (0.2%)

Table 3: Estimated values and associated uncertainties of the Mualem-van Genuchten model parameters for hydraulic conductivity of compost, pozzolan and effective material.

516 by dissolved gas entrapped in lava during scoria emission. The mineralogy of
517 rocks, the proportion of dissolved gas and the temperature of scoria during
518 volcanic eruption, all affect upon the porosity and pore size distribution of
519 pozzolan rocks.

520 Experimental data were less spread out for the water retention of bark
521 compost. Contrary to pozzolan, the water retention measurements for bark
522 compost were obtained on remolded, compacted samples. The porosity of
523 compacted bark compost includes both the matric porosity of individual
524 bark fragments and the structural porosity between bark fragments. As ob-
525 served for natural soils [47], water retention near saturation was related to
526 structural porosity. We found a very good linear relationship between water
527 retention data and apparent bulk density for matric potentials greater than
528 -0.7 m (data not shown). Consequently, variability in the water retention
529 measurements was very low near saturation, since the apparent bulk density
530 of bark compost samples was accurately controlled. For lower matric poten-
531 tial values, the variability was due to the variability of matric porosity and
532 pore size distribution of bark fragments. This experimental dispersion was
533 relatively low, since the highest standard deviation value was $0.02 \text{ m}^3/\text{m}^3$.

534 Figs. 2 show that in all the cases studied, the van Genuchten model ade-
535 quately fitted water retention experimental data. The estimated uncertainty
536 distributions had a similar behaviour to those of the experimental ones: a

537 lower level of uncertainty for compost than for pozzolan, particularly for ma-
538 tric potentials between -0.01 m and -1 m, and a higher level of uncertainty
539 near saturation. The higher level of uncertainty in the water retention values
540 for compost near saturation was not due to greater experimental uncertain-
541 ties, as was the case for pozzolan, but due to a lack of experimental data.
542 For both materials, the most variable and least variable parameter, respec-
543 tively, were h_e and the n exponent, with respective coefficient of variations
544 of approximately 20% and 1 % for bark compost data, and 35% and 1 %
545 for pozzolan aggregates data (see Table 2). The h_e parameter is a scale pa-
546 rameter which is related to the entry point of air into the studied material,
547 whereas the n parameter is a shape parameter related to the pore size distri-
548 bution [34]: a greater scattering of the h_e parameter could, thus, be linked
549 to the macroporosity variability. A slight variability in the exponent n was
550 representative of a homogeneous meso- and micro-pore size distribution for
551 both materials.

552 *4.1.2. Comments on the hydraulic conductivity results*

553 The K_{Sat} experimental values ranged from 10^{-7} to 10^{-3} m.s $^{-1}$ for poz-
554 zolan samples. The conductivities at saturation of “porous” blocks were
555 higher than those of “dense” blocks (not shown here). The relative standard
556 deviation of K_{Sat} was relatively low for compost. This was expected as was
557 previously explained in section 2.5, and substantiated the fact that only a
558 single sample was used for determining of the hydraulic properties of bark
559 compost. For the unsaturated part of the hydraulic conductivity curve, the
560 experimental scattering of (K, h) data found for pozzolan and bark compost
561 materials were similar to the scattering of data found for natural soils using
562 the Wind evaporation method [28]. In Figs. 3, data obtained for pozzolan
563 samples are represented with the same symbol since experimental scattering
564 largely overlaps from one sample to the other. We observed a lack of exper-
565 imental values between the data obtained under saturated and unsaturated
566 conditions. This is due to the limited accuracy of matric potential sensors
567 and to the Wind evaporation method: it is necessary to have significant
568 matric potential gradients between two successive sensors to compute an ac-
569 curate value of the unsaturated hydraulic conductivity, and this is usually
570 not achieved close to saturation [28]. Despite this limitation, direct compu-
571 tation of K values could be obtained using the Wind evaporation, which is
572 not the case for inverse methods used either in the onestep or the multistep
573 outflow methods [48] where only curve parameters are fitted.

574 Figs. 3 show that, as expected, the estimated uncertainty of the hydraulic
 575 conductivity of pozzolan was greater than that of bark compost. The uncer-
 576 tainty distribution of parameter n was very low for both materials (see Table
 577 3). For the h_e and K_{sat} parameters, the scattering was greater for pozzolan
 578 material than for bark compost material.

579 4.2. Effective water retention and hydraulic conductivity curves

580 Various analytical bounds or estimations for effective hydraulic conduc-
 581 tivities can be found in the literature [9] [49]. The Wiener bounds give a
 582 fundamental inequality which is always valid. Let $\mu_{a|K}$ and $\mu_{h|K}$ be the
 583 arithmetic and harmonic means of conductivity values, ω_C and ω_P the volu-
 584 mic proportion of each material, and K_C and K_P the hydraulic conductivities
 585 of compost and pozzolan, respectively. For each water matric potential h ,
 586 the effective conductivity K_{eff} can be bounded as follows

$$\mu_{h|K} = \frac{1}{\omega_C/K_C + \omega_P/K_P} \leq K_{eff} \leq \mu_{a|K} = \omega_C K_C + \omega_P K_P$$

587 Note that the Wiener bounds presuppose a plane layered structure of
 588 the medium. The harmonic and arithmetic means are obtained, respectively,
 589 when the water flux is perpendicular or parallel to the main orientation of the
 590 layered surface. For a statistically homogeneous and isotropic medium, [49]
 591 proposed an estimation of the effective conductivity calculated by a geometric
 592 weighted average of the arithmetic and harmonic means $\mu_{a|K}$ and $\mu_{h|K}$. This
 593 curve, designed as the Matheron curve in the following sections, is defined
 594 by $\mu_{M|K} = \mu_{a|K}^\alpha \mu_{h|K}^{1-\alpha}$, where $\alpha = (D - 1)/D$ and D is the dimension of the
 595 problem.

596 For effective water retention, an analytical estimation was simply ob-
 597 tained by the addition of the water retention properties for each component,
 598 taking into account their respective proportions.

599 Figs. 4 show the means and standard deviations of effective conductiv-
 600 ity values obtained as described in section 3.2, as well as the means of the
 601 corresponding Wiener bounds and Matheron estimations. The means of the
 602 effective conductivity values, for each water matric potential value, must be
 603 included into the means of the corresponding Wiener bounds. The crosses
 604 which can be observed in Figs. 4 are well-bounded, validating the numerical
 605 procedure developed to determine the effective values. Note that the means
 606 of the effective conductivity values are closer to the arithmetic mean curve.
 607 They are above the Matheron mean curve before the intersection between the

608 Wiener curves, and below after that intersection. Fig. 5 presents the means
609 and standard deviations of the effective retention values. The effective water
610 retention values computed correspond to the arithmetic mean curve. This
611 result was already obtained by several authors, see [13] [14] citevogel2008
612 among others. Under quasi static conditions and without dynamic effects,
613 the water retention curve presents a capacitive property [25] and the effective
614 water retention curve can be calculated from the additive properties of the
615 local water retention curves [14]. The standard deviations of the effective
616 conductivity and retention values computed for the four water potential val-
617 ues were between those obtained for bark compost and pozzolan, and close
618 to the standard deviation of their arithmetic means (results not shown).

619 The uncertainty distributions of the effective water retention and the
620 hydraulic conductivity are presented in Figs. 6. Estimated values and stan-
621 dard deviations for the corresponding parameters of the van Genuchten and
622 Mualem-van Genuchten models are displayed in Tables 2 and 3.

623 The estimated uncertainties for the effective conductivity and water re-
624 tention parameters were relatively low and generally inferior to those of bark
625 compost and pozzolan, under unsaturated conditions. This was mainly due
626 to the size (number of replicates \times number of water potential values), and
627 to a lower extent, given this size, to the optimal choice of the numerical ex-
628 perimental design used for computing the effective conductivity and water
629 retention values from those measured for bark compost and pozzolan. These
630 uncertainties increased closer to saturation following the same trend as the
631 one observed for individual components. The standard deviations of most
632 of the van Genuchten and Mualem-van Genuchten parameters estimated for
633 the effective material were lower than the ones estimated for bark compost
634 and pozzolan. The standard deviations of the parameters, directly linked to
635 saturated conditions (K_{Sat} and θ_s) estimated for the effective material, were
636 between those estimated for bark compost and pozzolan. To conclude this
637 section, the proposed methodology applied using an optimal sampling design
638 led to “well defined” effective properties. This means that (i) the effective
639 properties of the composite substrate could be calculated from the proper-
640 ties of each material and their relative proportion in the composite substrate,
641 and that (ii) the uncertainties of the effective properties were lower than the
642 uncertainties of the properties of each material. The reduction in the level of
643 uncertainty was more pronounced for the van Genuchten parameters associ-
644 ated to the dry part of the properties (θ_r, h_e, n) than for the ones associated
645 to the wet part of the properties (θ_s, K_{sat}).

646 *4.3. Evaluation of the upscaling approach under dynamic evaporation*

647 Three snapshots of water potential values obtained at different simulation
648 time points during the evaporation process are presented in Figs. 7 for the
649 bimaterial configuration. Heterogeneous spatial distributions of these values
650 were observed at the upper surface of the soil core at $t = 2$ days and $t = 6$
651 days. Blue shades represent the gradients due to the geometrical distribution
652 of the two materials. Consequently, isovalues of h did not correspond to
653 horizontal planes. At $t = 10$ days, the Dirichlet condition replaced the flux
654 condition at the upper surface, which led to a uniform spatial distribution of
655 water matric potential values at $z = 0$. A gradually stronger vertical gradient
656 could be seen in-depth as evaporation took place.

657 Figs. 8 present the uncertainty distributions of water matric potential
658 mean values per depths for the evaporation process and for the bimaterial
659 configuration and the corresponding effective homogeneous material configura-
660 tion. The uncertainty distributions obtained for the effective homogeneous
661 material configuration were clearly less scattered than those obtained for the
662 bimaterial configuration and were included in their [25th, 75th] percentile
663 ranges (not shown here). This was a direct consequence of the lower level
664 of the uncertainties of the effective hydraulic properties of the material com-
665 pared to those of compost and pozzolan.

666 The means of these uncertainty distributions for each time point, simula-
667 tion configurations and depths are also presented in Figs. 8. The curves ob-
668 tained for the effective homogeneous material and the explicit two-component
669 medium were similar. This confirms the validity of the upscaling approach
670 in our study. However, some discrepancies appeared as simulation time in-
671 creased. Table 4 shows the mean water matric potential values and the mean
672 water content values for both configurations at $t_{max} = 10$ days, the final time
673 point of the evaporation simulation. Table 4 shows the water matric potential
674 means for each depth, and taking into account all of the uncertainties. Rela-
675 tive differences between the bimaterial configuration and the corresponding
676 effective homogeneous material configuration were relatively high for water
677 matric potentials, and were more pronounced in-depth. However, these rela-
678 tive differences concerned an area of the core where the porous media were
679 quite dry. Water content values of both the bimaterial and the homogeneous
680 material configurations were computed from these water matric potentials
681 using the van-Genuchten model and the parameters estimated for the ef-
682 fective material configuration given in Table 2. These water content values
683 presented in Table 4 show only slight differences between the two configura-

		Depth= -0.2 cm	Depth= -1.1 cm	Depth= -4.8 cm
Water matric potential means	Effective homogeneous material configuration	-45.78	-15.33	-5.68
	Bimaterial configuration	-53.71	-21.47	-8.36
	Relative differences	14.8%	28.6%	32.1%
Water content means	Effective homogeneous material configuration	7.81 e-2	9.12 e-2	10.69 e-2
	Bimaterial configuration	7.65 e-2	8.68 e-2	10.00 e-2
	Relative differences	2.1%	4.9%	6.4%

Table 4: Means of all water matric potential and water content values for several depth and for the bimaterial and effective material configurations.

684 tions, and the relative differences (between 2.1% and 6.4% at 10 days) are
685 lower than those of the water matric potentials.

686 Discrepancies may be due to the non-equilibrium flow process, a con-
687 sequence of the occurrence of transient processes during the dynamic sim-
688 ulation. Results obtained by [26] showed that modeling a non-equilibrium
689 flow modifies the dynamic response for infiltration scenarios, but hardly af-
690 fects the dynamic response for evaporation scenarios. During the evaporation
691 simulation, the average macroscopic flux was a vertical upward flux. How-
692 ever, the orientation of the local, microscopic water flux could be derived
693 from the vertical direction, due to the presence of local heterogeneous water
694 potential gradients as shown in Figs. 7. The tortuosity of the water flow
695 was, thus, increased. This local tortuosity is a kind of balance between the
696 boundary conditions leading to a vertical macroscopic flux and the contrast
697 of the hydraulic properties of both materials leading to the multidimension-
698 al microscopic water flux. The contrast of the hydraulic properties depends
699 on the local water content or matric potentials, and as these variables were
700 time dependent during the dynamic simulation, the tortuosity was also time
701 dependent. This time-dependent tortuosity was not accounted for during
702 the upscaling process since the determination of the effective properties was
703 performed under successive states of equilibrium, see section 3.2. As a conse-

704 quence of this time dependency of the local tortuosity, the overall evaporation
705 process of the heterogeneous medium could be accelerated or slowed down
706 compared to the effective material. Therefore, more complex models includ-
707 ing non-equilibrium terms might be implemented to study their influence on
708 the dynamic response using the present configuration.

709 5. Conclusion

710 The hydraulic properties of the green roof substrate were studied at the
711 Darcy scale using two different approaches. The first methodological ap-
712 proach consisted in determining the water retention and hydraulic conduc-
713 tivity curves for the two components of the green roof substrate considered,
714 namely bark compost and pozzolan. Associated uncertainties were evaluated
715 using a bootstrap method. It was shown, on a virtual evaporation experiment
716 conducted using a heterogenous material combining both these components,
717 that the impact of these uncertainties on the simulated water matric potential
718 was high.

719 The second methodological approach consisted in considering the hetero-
720 geneous green roof substrate as an homogeneous material using an upscaling
721 method. Effective water retention and hydraulic conductivity curves were fit-
722 ted on values computed for several water matric potentials using numerical
723 steady-state scenarios on the considered heterogenous material. Associated
724 uncertainties of these properties were also evaluated taking into account the
725 uncertainties of the hydraulic properties of the two components of the het-
726 erogeneous material. To that effect, for each hydraulic property, N couples of
727 curves were sampled in the uncertainty distributions of the two components
728 in an independent way for a set of water matric potential values. N was set
729 at a high value, and the water matric potential values were optimally chosen.
730 We have shown, here, that this methodology led to very low levels of uncer-
731 tainties in the effective properties of the material. A direct consequence of
732 this approach was that the uncertainties of simulated water potential for the
733 effective homogeneous material were very low compared to those obtained
734 on the equivalent heterogeneous material. This has shown that the use of
735 effective properties for a heterogenous material reduced the impact of the
736 uncertainties in the properties of its components. This is of importance since
737 the uncertainties linked to the experimental disposal and to the variability of
738 the materials properties may be high, as shown in the first part of the study.
739 It must be noted that the level of uncertainty obtained here for the simu-

740 lation of water matric potential in the effective material under evaporation
741 conditions is not representative of the level of uncertainty expected on the
742 simulation of a real evaporation experiment. In this last case, other types
743 of uncertainties, such as uncertainties on initial and boundary conditions for
744 example, must be taken into account.

745 Although the level of uncertainties obtained on the simulations of the
746 water matric potential differed for the heterogeneous and effective materials,
747 their mean values were almost similar. This confirms the adequacy of the
748 upscaling approach, for the heterogeneous material and associated configura-
749 tion, used in this study. The slight discrepancies observed between these
750 means may be due to the absence of non-equilibrium term in the simulation
751 model used. This term could be included in the scope of future studies.

752 From a practical point of view, our results can help to improve the ther-
753 mal and hydraulic functioning of GRS. From the hydraulic point of view,
754 the proposed methodology can already be used for optimizing the hydraulic
755 properties of composite pozzolan-bark compost substrate, in order to im-
756 prove the hydraulic functioning of green roof substrates (storm water man-
757 agement). When dealing with the thermal benefit for building equipped with
758 green roofs, many GRS parameters involved in the energy balance (thermal
759 conductivity, specific thermal capacity, albedo) at the roof surface vary as a
760 function of the GRS moisture content. Therefore the energy balance model
761 must be coupled with the water balance model of the GR. Effective para-
762 maters are needed for both models. The proposed methodology can thus also
763 be used to estimate the thermic effective parameters needed in the energy
764 balance model.

765 **6. Acknowledgment**

766 This work was supported by the French National Research Agency (ANR)
767 through the “Habitat intelligent et solaire photovoltaïque” program (project
768 AGROBAT ANR-09-HABISOL-001). We also thank the CINES (Centre
769 Informatique National de l’Enseignement Supérieur, France) for offering us
770 access to the supercomputer JADE to conduct these calculations successfully.
771 The authors wish to thank Profs. L. Di Pietro, G. Micolau, H. Bolvin and Dr.
772 C. Doussan for their helpful comments and careful readings of the manuscript.

- 773 [1] Yang J, Yu Q, Gong P. Quantifying air pollution removal by green
774 roofs in Chicago. *Atmos Environ* 2008;42(31):7266-7273.
- 775 [2] Rowe DB. Green roofs as a means of pollution abatement. *Environ*
776 *Pollut* 2011;159(8-9):2100-2110.
- 777 [3] Schrader S, Böning M. Soil formation on green roofs and its contri-
778 bution to urban biodiversity with emphasis on Collembolans. *Pedobiol*
779 2006;50(4):347-356.
- 780 [4] Hilten RN, Lawrence TM, Tollner EW. Modeling stormwater runoff
781 from green roofs with HYDRUS-1D. *J Hydrol* 2008;358(3-4):288-293.
- 782 [5] Czemieli Berndtsson J. Green roof performance towards management of
783 runoff water quantity and quality: A review. *Ecol Eng* 2010;36(4):351-
784 360.
- 785 [6] Lazzarin RM, Castellotti F, Busato F. Experimental measurements and
786 numerical modelling of a green roof. *Energy Build* 2005;37(12):1260-
787 1267.
- 788 [7] Feng C, Meng Q, Zhang Y. Theoretical and experimental analysis of the
789 energy balance of extensive green roofs. *Energy Build* 2010;42(6):959-
790 965.
- 791 [8] Jaffal I, Ouldboukhite SE, Belarbi R. A comprehensive study of the
792 impact of green roofs on building energy performance. *Renewable En-*
793 *ergy* 2012;43:157-164.
- 794 [9] Renard Ph, de Marsily G. Calculating equivalent permeability: a re-
795 view. *Adv Water Resour* 1997;20(5-6):253-278.
- 796 [10] Feyen J, Jacques D, Timmerman A, Vanderborght J. Modelling water
797 flow and solute transport in heterogeneous soils: a review of recent
798 approaches. *J Agric Eng Res* 1998;70(3):231-256.
- 799 [11] Vogel HJ, Roth K. Moving through scales of flow and transport in soil.
800 *J Hydrol* 2003;272(1-4):95-106.
- 801 [12] Vereecken H, Kasteel R, Vanderborght J, Harter T. Upscaling hydraulic
802 properties and soil water flow processes in heterogeneous soils: a review.
803 *Vadose Zone J* 2007;6:1-28.

- 804 [13] Samouëlian A, Cousin I, Dagès C, Frison A, Richard G. Determining
805 the effective hydraulic properties of a highly heterogeneous soil horizon.
806 *Vadose Zone J* 2011;10(1):450-458.
- 807 [14] Samouëlian A, Vogel HJ, Ippisch O. Upscaling hydraulic conductivity
808 based on the topology of the sub-scale structure. *Adv Water Resour*
809 2007;30(5):1179-1189.
- 810 [15] Vogel HJ, Weller U, Ippisch O. Non-equilibrium in soil hydraulic mod-
811 elling. *J Hydrol* 2010;393(1-2):20-28.
- 812 [16] Vogel HJ, Roth K. A new approach for determining soil hydraulic func-
813 tions. *Eur J Soil Sci* 1998;49(4):547-556.
- 814 [17] Javaux M, Vanclooster M. Three-dimensional structure characterisa-
815 tion and transient flow modelling of a variably saturated heterogeneous
816 monolith. *J Hydrol* 2006;327(3-4):516-524.
- 817 [18] Mohrath D, Bruckler L, Bertuzzi P, Gaudu JC, Bourlet M. Error analy-
818 sis of an evaporation method for determining hydrodynamic properties
819 in unsaturated soil. *Soil Sci Soc Am J* 1997;61(3):725-735.
- 820 [19] Peters A, Durner W. Simplified evaporation method for determining
821 soil hydraulic properties. *J Hydrol* 2008;356(1-2):147-162.
- 822 [20] Coppola A, Basile A, Comegna A, Lamaddalena N. Monte Carlo anal-
823 ysis of field water flow comparing uni- and bimodal effective hydraulic
824 parameters for structured soil. *J Contam Hydrol* 2009;104(1-4):153-165.
- 825 [21] Christiaens K, Feyen J. Analysis of uncertainties associated with dif-
826 ferent methods to determine soil hydraulic properties and their prop-
827 agation in the distributed hydrological MIKE SHE model. *J Hydrol*
828 2001;246(1-4):63-81.
- 829 [22] Pan F, Ye M, Zhu J, Wu Y-S, Hu B-X, Yu Z. Numerical evaluation
830 of uncertainty in water retention parameters and effect on predictive
831 uncertainty. *Vadose Zone J* 2009;8(1):158-166.
- 832 [23] Efron B, Tibshirani R. *An Introduction to the Bootstrap*. Boca Ra-
833 ton, FL: Chapman & Hall/CRC Monographs on Statistics & Applied
834 Probability;1993.

- 835 [24] Manly BFJ. Randomization, Bootstrap and Monte Carlo Methods in
836 Biology. Boca Raton, FL: Chapman & Hall/CRC;2007.
- 837 [25] Vogel H-J, Samouelian A, Ippisch O. Multi-step and two-step experi-
838 ments in heterogeneous porous media to evaluate the relevance of dy-
839 namic effects. *Adv Water Resour* 2008;31(1):181-188.
- 840 [26] Šimůnek J, Wendroth O, Wypler N, van Genuchten Mth. Non-
841 equilibrium water flow characterized by means of upward infiltration
842 experiments. *Eur J Soil Sci* 2001;52(1):13-24.
- 843 [27] Anonymous. www.fll.de. Guidelines for the planning, execution and
844 upkeep of green-roof sites. Bonn:FLL Ed;2002.
- 845 [28] Tamari S, Bruckler L, Halbertsma J, Chadoeuf J. A simple method
846 for determining soil hydraulic properties in the laboratory. *Soil Sci Soc
847 Am J* 1993;57(3):642-651.
- 848 [29] Dane JH, Hopmans JW. Method of Soil analysis - Part 4 Physical
849 Method. In: Dane JH, Topp GC, editors. *Water retention and storage*,
850 Madison:SSSA book series;2002.
- 851 [30] Monnier G, Stengel P, Fiès J-C. Une méthode de mesure de la densité
852 apparente de petits agglomérats terreux. Application à l'analyse des
853 systèmes de porosité du sol. In: *Annales Agronomiques*;1973.
- 854 [31] van Genuchten MTh. A closed-form equation for predicting the
855 hydraulic conductivity of unsaturated soils. *Soil Sci Soc Am J*
856 1980;44(5):892-898.
- 857 [32] Coleman TF, Li Y. An Interior, Trust Region Approach for Nonlinear
858 Minimization Subject to Bounds. *SIAM J. Optim* 1996;(6):418-445.
- 859 [33] Chossat JC. La mesure de la conductivité hydraulique dans les sols -
860 Choix des méthodes. Paris:Tec et Doc Ed - Lavoisier;2005.
- 861 [34] Kutilek M, Nielsen DR. *Soil Hydrology*. Catena Verlag;1994.
- 862 [35] Celia MA, Bouloutas ET, Zarba RL. A general mass-conservative nu-
863 merical solution for the unsaturated flow equation. *Water Resour Res*
864 1990;26(7):1483-1496.

- 865 [36] Renaud J, Cloke H, Wang Y, Anderson M, Wilkinson P, Lloyd D.
866 Simulation numérique d'écoulements en milieu poreux avec l'équation
867 de Richards. *Eur J Comput Mech* 2003;12(2-3):203-220.
- 868 [37] Kavetski D, Binning P, Sloan SW. Adaptive time stepping and error
869 control in a mass conservative numerical solution of the mixed form of
870 Richards equation. *Adv Water Resour* 2001;24(6):595-605.
- 871 [38] Dhatt G, Touzot G, Lefrancois E. *Méthode des éléments finis*. Lon-
872 don:Hermes Science Publications - Lavoisier;2004.
- 873 [39] Ju SH, Kung KJS. Mass types, element orders and solution schemes
874 for the Richards equation. *Comput Geosci* 1997;23(2):175-187.
- 875 [40] Huang K, Mohanty BP, van Genuchten MTh. A new convergence cri-
876 terion for the modified Picard iteration method to solve the variably
877 saturated flow equation. *J Hydrol* 1996;178(1-4):69-91.
- 878 [41] Tracy FT. Three-dimensional analytical solutions of Richards' equation
879 for a box-shaped soil sample with piecewise-constant head boundary
880 conditions on the top. *J Hydrol* 2007;336(3-4):391-400.
- 881 [42] Fityus SG, Smith DW. Solution of the unsaturated soil moisture equa-
882 tion using repeated transforms. *Int J Numer Anal Methods Geomech*
883 2001;25(15):1501-1524.
- 884 [43] Vanderborght J, Kasteel R, Herbst M, Javaux M, Thiéry D, Van-
885 clooster M, Mouvet C, Vereecken H. A set of analytical benchmarks
886 to test numerical models of flow and transport in soils. *Vadose Zone J*
887 2005;4(1):206-221.
- 888 [44] Hardelauf H, Javaux M, Herbst M, Gottschalk S, Kasteel R, Vander-
889 borght J, Vereecken H. PARSWMS: A parallelized model for simulating
890 three-dimensional water flow and solute transport in variably saturated
891 soils. *Vadose Zone J* 2007;6(2):255-259.
- 892 [45] Herbst M, Gottschalk S, Reissel M, Hardelauf H, Kasteel R, Javaux M,
893 Vanderborght J, Vereecken H. On preconditioning for a parallel solution
894 of the Richards equation. *Comput Geosci* 2008;34(12):1958-1963.

- 895 [46] Atkinson AC, Donev AN. Optimum experimental designs. Ox-
896 ford:Clarendon Press;1992.
- 897 [47] Dexter AR, Czyz EA, Richard G, Reszkowska A. A user-friendly water
898 retention function that takes account of the textural and structural
899 pore spaces in soil. *Geoderma* 2008;143(3-4):243-253.
- 900 [48] Hopmans JW, Simunek J, Romane N, Durner W. Method of Soil anal-
901 ysis - Part 4 Physical Method. In: Dane JH, Topp GC editors. Simul-
902 taneous determination of water transmission and retention properties
903 - Inverse methods, Madison:SSSA book series;2002.
- 904 [49] Matheron G. *Éléments pour une Théorie des Milieux Poreux*.
905 Paris:Masson et Cie;1967.

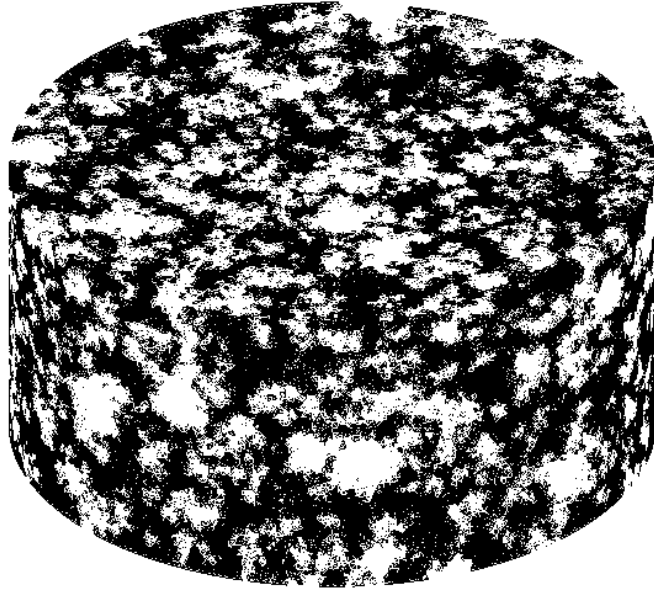
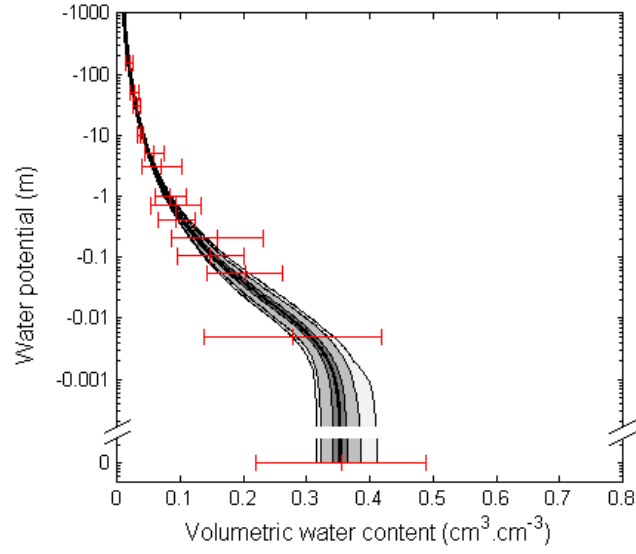
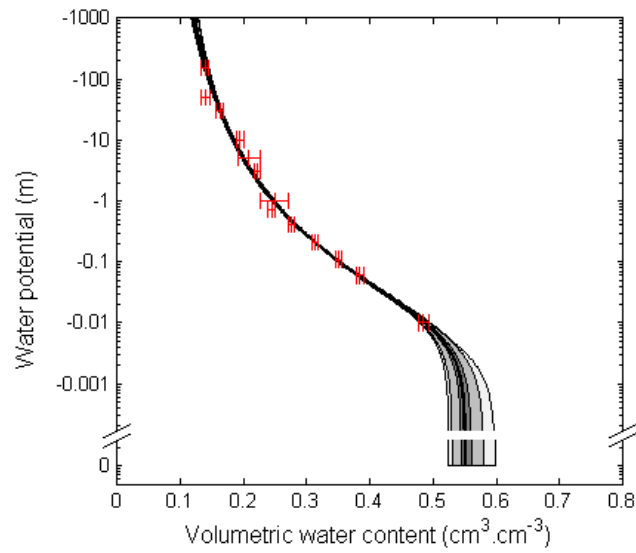


Figure 1: Typical heterogeneous mesh for the bimaterial configuration. Black or white zones correspond, respectively, to the pozzolan or bark compost component.

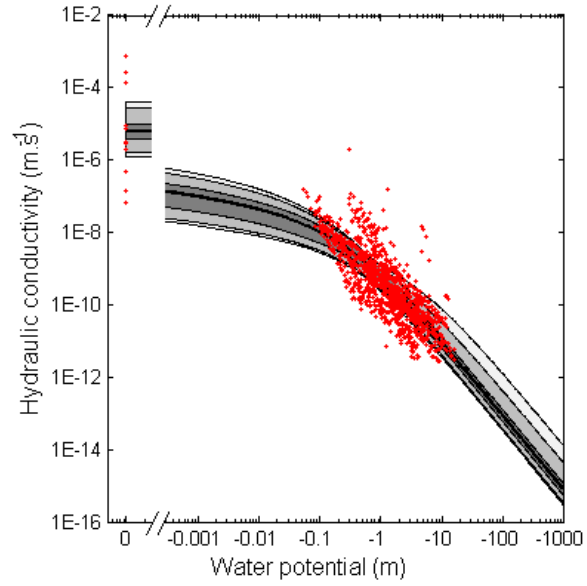


(a)

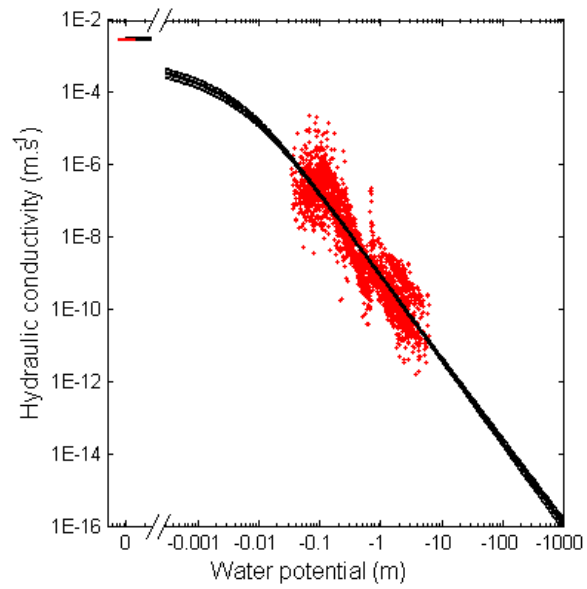


(b)

Figure 2: Uncertainty distributions of a) pozzolan and b) compost water retention values. Crosses and error bars represent means and ± 1 standard deviations of measured data and curves represent 0.5, 2.5, 25, 75, 97.5, 99.5 percentiles and median of the estimated water retention uncertainty distributions. Vertical axes are in log scale.

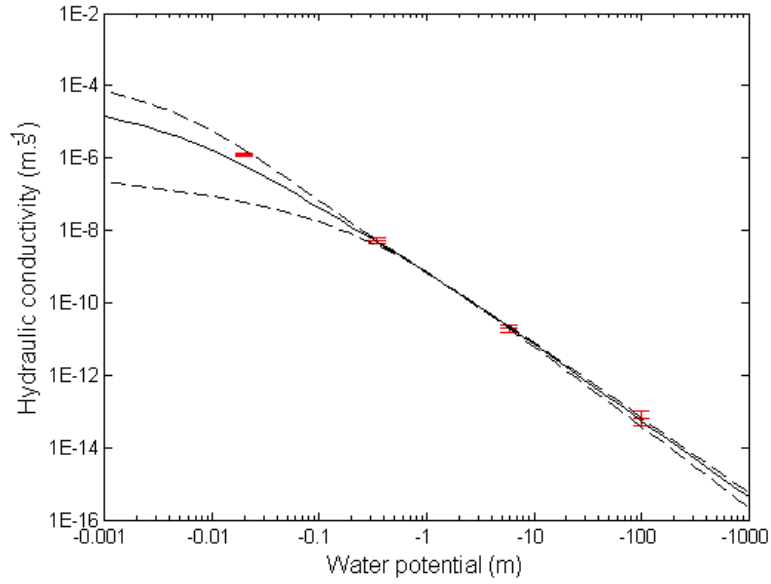


(a)

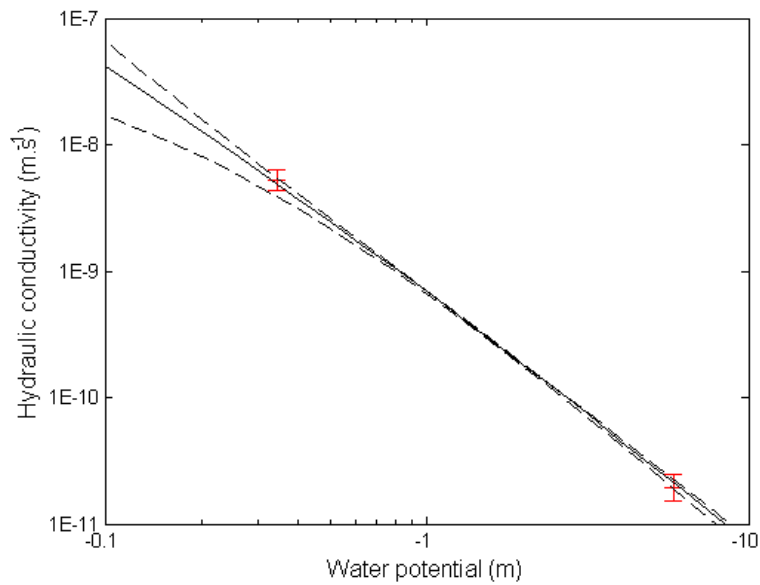


(b)

Figure 3: Uncertainty distributions of a) pozzolan and b) compost hydraulic conductivity values. Crosses represent measured data and curves represent 0.5, 2.5, 25, 75, 97.5, 99.5 percentiles and median of the estimated hydraulic conductivity distributions. Vertical and horizontal axes are in log scale.



(a)



(b)

Figure 4: Effective conductivity values computed from 200 compost and pozzolan properties for 4 water matric potential values. Crosses represent the mean and ± 1 standard deviations of the 50 computed values per water matric potential point, dotted lines are the means of the Wiener bounds and the plain line is the Matheron curve obtained from these mean curves. Fig. b) is an enhanced view of Fig. a). Vertical and horizontal axes are in log scale.

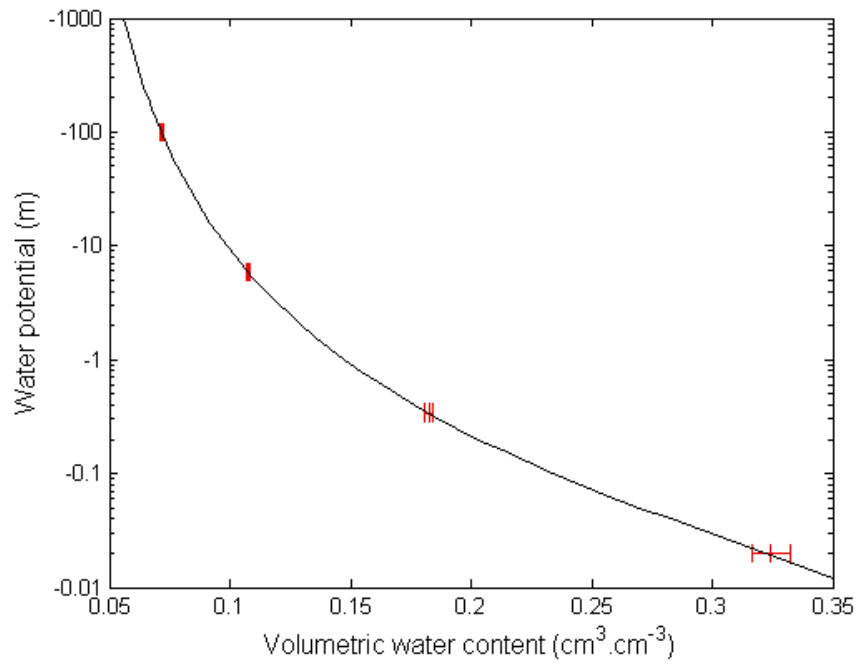
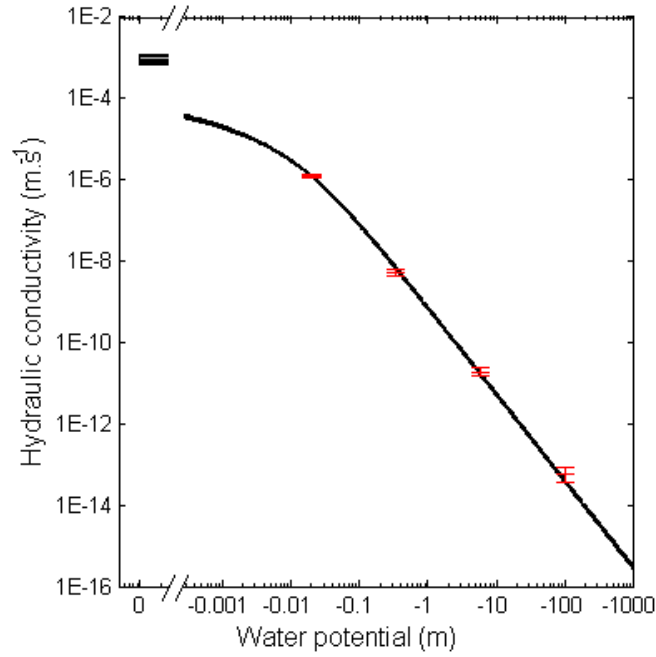
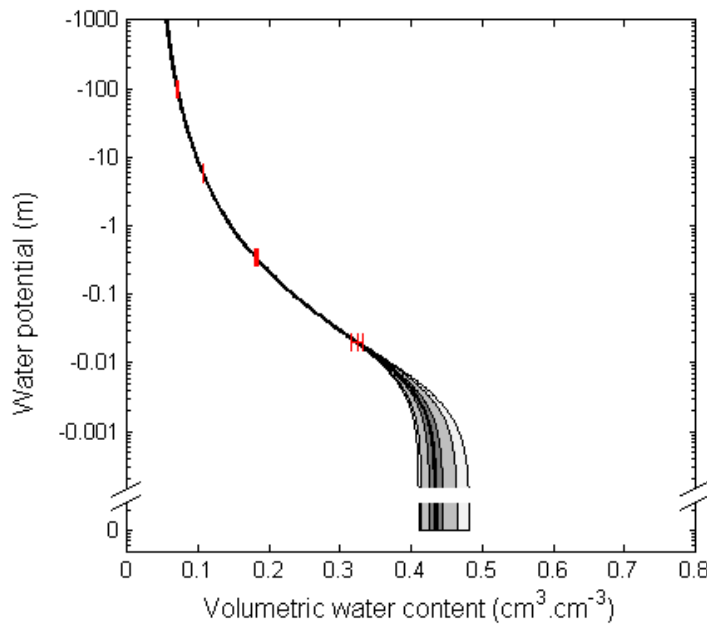


Figure 5: Effective retention values computed from 200 compost and pozzolan properties for 4 water matric potential values. Crosses represent the mean and ± 1 standard deviations of the 50 computed values per water matric potential point and the plain line is the mean of the arithmetic mean curves obtained from the compost and pozzolan retention curves used. The horizontal axis is in log scale.

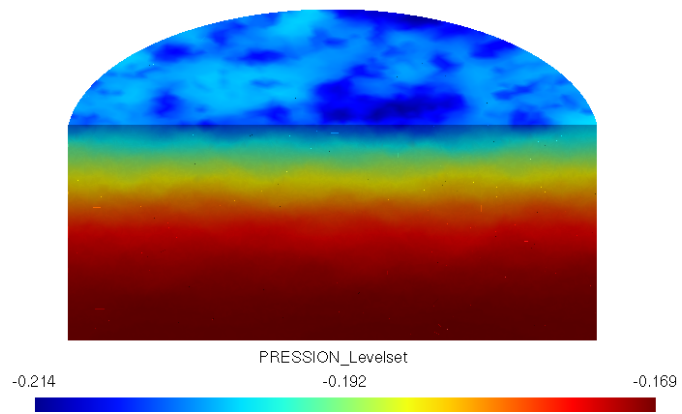


(a)

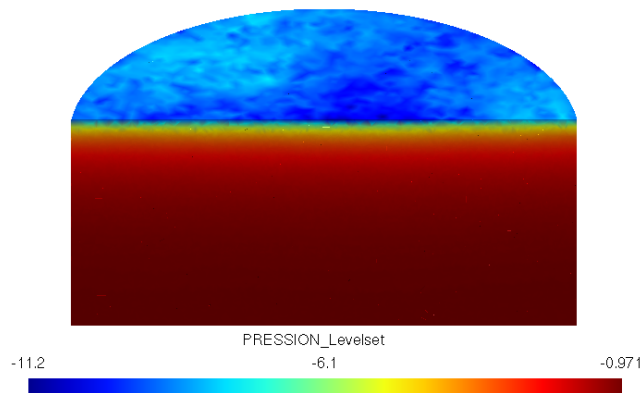


(b)

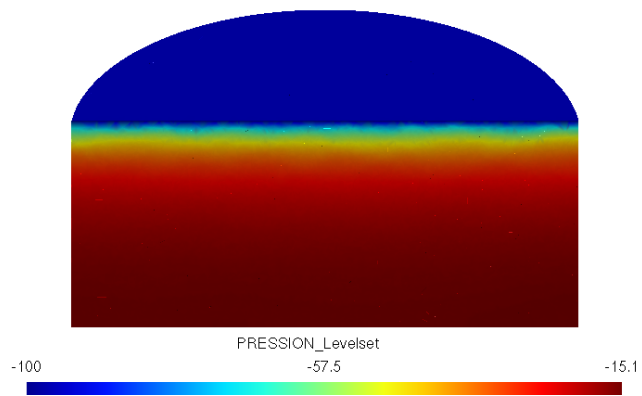
Figure 6: Uncertainty distributions of a) effective hydraulic conductivity and b) water retention. Crosses and error bars represent means and ± 1 standard deviations of simulated data and curves represent 0.5, 2.5, 25, 75, 97.5, 99.5 percentiles and median of the estimated hydraulic conductivity and water retention distributions. The vertical axes are in log scale. The horizontal axis of plot a) is also in log scale.



(a)



(b)



(c)

Figure 7: Snapshots of the evolution of the water potential according to time, at a) $t = 2$ days, b) $t = 6$ days and c) $t = 10$ days. Scales for water matric potential are different for each snapshot.

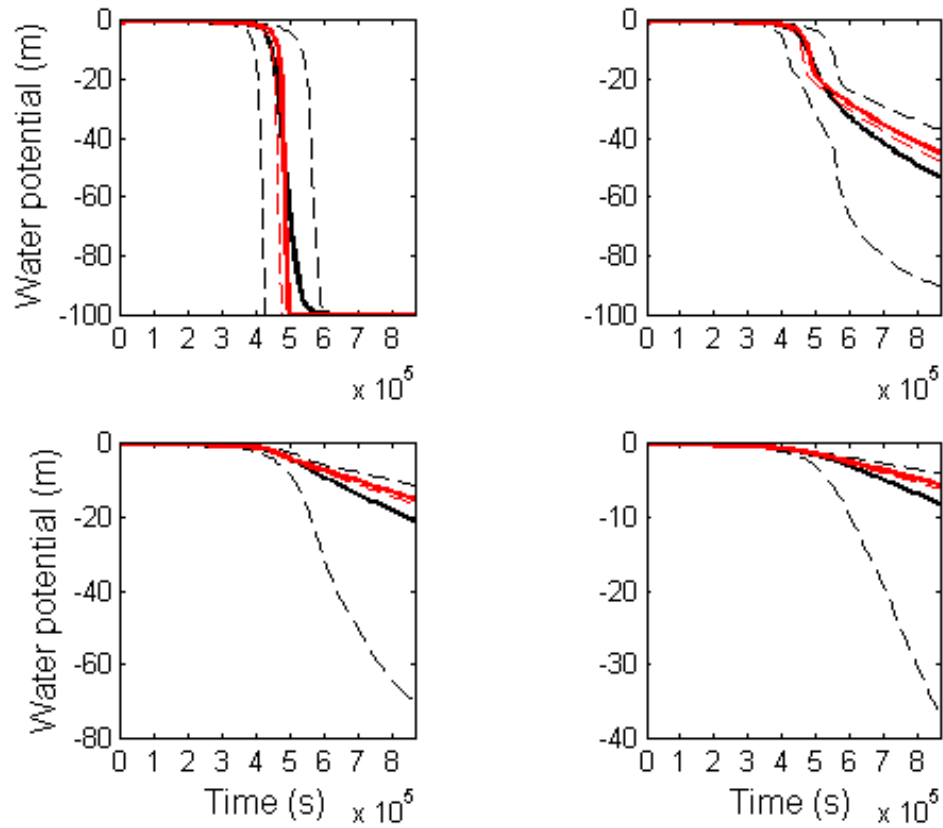


Figure 8: Uncertainty distributions of water matric potential values obtained by simulating evaporation using the heterogeneous green roof substrate (black curves) and using the corresponding computed effective homogeneous material (red curves). Dotted or solid curves represent, respectively, 0.5, 99.5 percentile or median values for the water matric potential distributions. The 4 graphs correspond to 4 various depths of the core.